Available online at www.sciencedirect.com
ScienceDirect
Corrosion Science 49 (2007) 4202–4231
CORROSION SCIENCE
www.elsevier.com/locate/corsci

Study of iron benzoate as a novel steel corrosion inhibitor pigment for protective paint films

G. Blustein [a], A.R. Di Sarli [a], J.A. Jaén [b], R. Romagnoli [a], B. Del Amo [a,*]

[a] *CIDEPINT – Centro de Investigación y Desarrollo en Tecnología de Pinturas (CICPBA-CONICET), Calle 52 el 121 y 122 (B1900AYB) La Plata, Argentina*
[b] *Departamento de Química Física, Facultad de Ciencias Naturales, Exactas y Tecnología, Universidad de Panamá (0834-00900) Panamá, Panama*

Received 9 August 2006; accepted 16 May 2007
Available online 8 June 2007

Abstract

The aim of this work was to study the lab-synthesized iron benzoate as a novel steel corrosion inhibitor pigment to formulate anticorrosive paint films. The iron benzoate anticorrosive properties were studied by electrochemical and spectroscopic essays employing pigment suspensions. In a second stage, it was evaluated the performance of anticorrosive paint films containing iron benzoate by accelerated (salt spray and humidity chambers) and EIS tests. The protective layer nature grown under the paint films in the salt spray chamber was also assessed.

Experimental results shown that ferric benzoate was adequate to formulate anticorrosive paint films with improved anticorrosive assessed.

Keywords: A. Steel; B. Mössbauer spectroscopy; B. EIS; B. Polarization; C. Paint coatings; C. Passive films

1. Introduction

Organic coatings are commonly used to protect metals against corrosion. It is estimated that about 85% of metal structures, exposed to different aggressive environments, are

* Corresponding author. Tel.: +54 221 4831141/44; fax: +54 221 4271537.
E-mail address: pinturashigienicas@cidepint.gov.ar (B. Del Amo).

0010-938X/$ - see front matter © 2007 Elsevier Ltd. All rights reserved.
doi:10.1016/j.corsci.2007.05.008

painted. Usually, inorganic crystalline solids are used as pigments, one of the basic components of primer formulations. They can play different roles such as colour supplying or enhance chemical or physical strength of the paint. Other pigments act as inhibitors increasing the anticorrosive resistance of metals. Chemically active pigments dissolve continuously in the water permeating through the organic coating and form an inhibitive solution that reaches the metal/coating interface and influences the electrochemical reactions. Among this kind of pigments, the most extensively used were red lead oxide and zinc chromate due to their efficiency. However, these compounds are highly toxic and cause severe environmental pollution. In recent decades, environmentally friendly pigments for primers formulation have been proposed as an alternative to traditional anticorrosive pigments. Zinc phosphate was the first but many other pigments were developed.

The inhibitive properties of a given pigment depend on the nature of the anion and/or the cation. In this sense, the inhibitive properties of benzoate anion were known from many years ago and were studied employing sodium benzoate and benzoic acid, in different media, still those containing chloride [1–15]. The employment of benzoate anion in combination with other anions such as gluconates was also reported [16] and, more recently, the inhibitive properties of calcium benzoate in neutral media were studied [17]. Sodium benzoate and benzoic acid were used as corrosion inhibitors not only for ferrous substrates but also for other metals [18–25]. The mechanism of the anticorrosive action of benzoates involves the anion adsorption onto the active sites of the metallic surface which provides an effective coverage and, consequently, corrosion rate decrease [16,26,27].

Soluble salts of benzoic acid were also employed in concrete [28,29] and in the field of paint technology. In this last case, they were used as soluble inhibitive additives in anticorrosive coatings and as active insoluble pigments in antifouling paints [30–38].

The employment of soluble compounds (benzoic acid, sodium benzoate, etc.) in anticorrosive paints is limited by the fact that their lixiviation, by water penetrating the pores of the coating, would greatly increase its permeability with the concomitant loss of the protective properties of the paint. However, it is possible to prepare insoluble metallic benzoates with certain cations (iron, zinc, aluminium, etc.) whose compounds are widely used in paint technology.

The aim of this research work was to study the inhibitive properties of ferric benzoate in paints. The pigment was precipitated under defined conditions and its anticorrosive properties were investigated by means of electrochemical techniques in pigment suspensions. In a second stage, anticorrosive paints containing ferric benzoate were formulated and their performance was evaluated by accelerated (salt spray and humidity chambers) and electrochemical (EIS) tests.

2. Experimental section

2.1. Pigment preparation and characterization

The solution-precipitate equilibrium between ferric cation and benzoate anion was studied in order to find the most suitable conditions to precipitate ferric benzoate and to determine the solubility of this compound. In this sense, the titration of each reactant (benzoic acid and ferric ion) and the titration of a solution containing both ions, with standardized sodium hydroxide, was carried out, at constant temperature (25 °C).

The solubility product constant (K_{SP}) of ferric hydroxide must be determined firstly in order to obtain K_{SP} of ferric benzoate. This was accomplished by titrating 5.00 mL of 0.1019 M ferric nitrate, acidified with 15.00 mL of 0.1065 M hydrochloric acid, in the absence of sodium benzoate and in the presence of 75.00 mL of 0.0188 M sodium benzoate. The final volume in the titration cell was kept constant in all cases. The titration of benzoic acid was also carried out to obtain the acid constant in the reaction medium employed in this research. The titrating solution was 0.1253 M sodium hydroxide. Reagent grade chemicals were used in all cases.

As it will be discussed later, titration curves showed the advantage of preparing ferric benzoate starting from 1.00 M ammonium benzoate and 0.33 M ferric nitrate. The ferric nitrate solution was dropped into a beaker containing 1 L of the benzoate solution, under continuous stirring. Once the addition of ferric nitrate was completed, the solution was stirred during one hour. The precipitate was washed three times with 10^{-3} M ammonium benzoate to avoid its hydrolysis; the supernatant liquid was then decanted. Finally, the precipitate was filtered through a Büchner funnel and dried at 50 °C until constant weight.

The precipitate stoichiometry was determined weighting 0.2500 g of the precipitate and dissolving it in 180 mL of distilled water plus 20 mL H_2SO_4 1:1. The resulting solution was heated gently until complete dissolution was accomplished, cooled down to room temperature and placed in a 250 mL volumetric flask. An aliquot of 10 mL was treated with 5 mL of 1.000 N $K_2Cr_2O_7$ plus 30 mL of concentrated H_2SO_4 and allowed to react for one hour at 50 °C in order to determine the benzoate content in the precipitate. Then, 100 mL of distilled water was added to the beaker and the excess of potassium dichromate was back titrated with 0.5000 N $FeSO_4$ in phosphoric medium, using a potentiometric technique with platinum electrodes polarized with 5 μA. Iron was determined by indirect gravimetry, weighting 1.0000 g of ferric benzoate into a crucible. The sample was dried at 50 °C and then burned at 1100 °C.

Physicochemical properties of the pigment, relevant to paint technology, such as density (ASTM D 1475) and oil absorption (ASTM D 281), were measured, according to standardised procedures, in order to sketch a correct paint formulation.

The pigment inhibitive properties were evaluated by means of electrochemical techniques, employing SAE 1010 steel electrodes with low surface roughness (mean peak-to-valley height 1.40 μm). The corrosion potential was monitored, as a function of time, against a saturated calomel electrode (SCE). The supporting electrolyte was a pigment suspension in 0.025 M sodium perchlorate. Sodium perchlorate solution was chosen as supporting electrolyte, in these preliminary studies, to avoid the intense attack produced by chloride which makes impossible to observe the different processes which take place during corrosion. However, final essays on painted steel were carried out with both electrolytes. Electrochemical tests were also performed in suspensions containing zinc oxide, which was employed to increase the pH of the ferric benzoate suspension (3.58) to achieve pH values for which the passivation of the substrate could be possible [39]. Zinc oxide is a complementary pigment commonly added to paints formulation [40].

The protective layer morphology formed on steel, at the open circuit potential, was studied by Scanning Electron Microscopy (SEM) employing a PHILLIPS SEM 505 coupled with an EDAX OX PRIME 10 (Energy dispersed form) to determine the surface elemental composition.

Steel corrosion rates, in pigment suspension in 0.5 M sodium perchlorate, at different exposure times, were obtained from polarisation resistance measurements. A SCE and a

platinum grid were used as reference and counter electrodes, respectively. The swept amplitude was ±0.250 V from the open circuit potential and the scan rate 0.250 mV s^{-1}. Measurements were carried out with a Potentiostat/Galvanostat EG&G PAR Model 273 A plus SOFTCORR 352 software.

Previous results showed the advantage of obtaining reaction products spectra from a mix of spectroscopic pure iron and ferric benzoate, molar ratio 1:1, which was wetted periodically with distilled water during a fortnight. The aim of this experiment was to identify the compounds responsible of the protection afforded by iron benzoate. Products identification was carried out via spectroscopic techniques: UV–visible diffuse reflectance, FTIR and Mössbauer.

The reflectance spectra were recorded with a GBC CINTRA 40/UV–VISIBLE SPECTROMETER. Spectra were scanned, at 50 nm min^{-1}, in the 200–800 nm range. FTIR spectra were obtained with a PERKIN ELMER RX1 SPECTROMETER. The Mössbauer spectrometer was a conventional one of constant acceleration with a $^{57}Co(Rh)$ source of 20 mCi.

2.2. Paints composition, manufacture and application

Three different paints were formulated, two of the solvent-borne type (alkyd and epoxy) and one epoxy water-borne paint.

The resins used to formulate solvent-borne paints were as follows: a medium oil alkyd (50% linseed oil, 30% *o*-phthalic anhydride, 8% pentaerythritol and glicerol and 12% pentaerythritol resinate) and a bisphenol epoxy-polyamide resin (1:1 ratio, by volume, v/v). The solvent employed in the former case was white spirit while the mixture xylene/methyl isobutyl ketone/butyl cellosolve (13/45/42%, by weight, w/w) was used for the epoxy paint. It was decided to check the anticorrosive properties of the pigment employing solvent-borne paints because their behaviour has been well documented for many years. The PVC/CPVC (pigment volume concentration/critical pigment volume concentration) relationship was 0.8 as suggested elsewhere [41].

The anticorrosive pigment load was 30% v/v of the total pigment content; the same value suggested when orthophosphates are employed as anticorrosive pigments [41,42]. Titanium dioxide, barium sulphate and talc were incorporated to complete the pigment formula. In order to achieve an acceptable dispersion degree [43], all the pigments were dispersed in the vehicle for 24 h by using a ball mill. Paints formulations are shown in Table 1.

An epoxy resin based on a mix of bisphenol A and bisphenol F was chosen to formulate water-borne paints. The curing agent (hardener), which also acts as emulsifier, was a modified polyamidoamine with 50% of solids. The resin/hardener ratio was 100/120 w/w. Neutral demineralized water was employed as solvent.

The anticorrosive pigment content was 30% of the total pigment content. Titanium dioxide, barium sulphate, talc and mica were incorporated to complete the pigment formula. Mica was added to the formulation due to its barrier properties and ability to reduce the "flash rusting" degree [44]. The PVC value (25%) was chosen in order to enhance the coatings barrier effect. Water-borne paint composition is also shown in Table 1.

Water-borne paint was prepared in a high-speed disperser. Preliminary tests showed the advantage of incorporating the pigment into the hardener, instead of mixing it with the resin. The relatively high viscosity of the hardener made it necessary to add, firstly,

Table 1
Paint composition as percentage of solids by volume

Components	Paints		
	1	2	3
Iron benzoate	13.6	13.6	3.5
Barium sulphate	12.5	12.5	2.2
Talc	12.5	12.5	2.1
Titanium dioxide	5.0	5.0	2.1
Ferric oxide	1.2	1.2	0.3
Mica	–	–	1.8
Epoxy resin/polyamide resin (1/1 ratio)	26.6	–	–
Alkyd resin	–	26.6	–
Hardener/resin (1.2/1 ratio)	–	–	65.8
Additives	–	–	1.5
Solvents	28.6	28.6	20.7
Anticorrosive pigment/total pigment (v/v)	30	30	30

the water and, then, the pigments in accordance with their increasing oil absorption index; mica was added at last to avoid the break-up of laminar particles.

SAE 1010 steel panels ($15.0 \times 7.5 \times 0.2$ cm) were sandblasted to Sa 2 1/2 (SIS 05 59 00), degreased with toluene and then painted by brushing to reach a dry film thickness of 80 ± 5 μm. Painted panels were kept indoors for 14 days before testing.

2.3. Study of paint anticorrosive performance through accelerated and electrochemical tests

A set of three panels painted with each paint type was placed in the salt spray chamber (ASTM B-117). Rusting (ASTM D-610) and blistering (ASTM D-714) degrees were evaluated during 4200 h of exposure. Wet adhesion was also determined according to a standard test (ASTM D 3359- method B).

After the exposure to the salt spray chamber, the coating on the steel panels was removed with suitable solvents. The morphology of the protective layer was observed by SEM, the surface elemental composition determined by EDAX and, finally, corrosion products were identified by UV–visible diffuse reflectance and FTIR Spectroscopy.

Another set of panels was placed in the humidity chamber, at 38 ± 1 °C (ASTM D 2247), for 4000 h. Rusting and blistering degrees were evaluated periodically, according to the above mentioned standard specifications.

Impedance spectra of painted panels (frequency range 1×10^{-3} Hz $\leqslant f \leqslant 1 \times 10^{5}$ Hz) were performed in the potentiostatic mode, at the corrosion potential. Measurements were done as a function of the exposure time to the electrolyte solutions (0.5 M $NaClO_4$ and 3% NaCl), using the 1255 Solartron FRA and the 1286 Solartron EI. The amplitude of the applied AC voltage was 0.010 V peak to peak. Two acrylic tubes were attached to each coated panel (working electrode) with an epoxy adhesive in order to perform the electrochemical measurements. The geometric area exposed to the electrolyte was 15.9 cm^2. A large area Pt–Rh mesh of negligible impedance and saturated calomel (SCE) were employed as auxiliary and reference electrodes, respectively. The experimental impedance spectra were interpreted on the basis of equivalent electrical circuits using a suitable fitting

procedure developed by Boukamp [45]. This electrochemical experiments were carried out at laboratory temperature (20 ± 2 °C) using a Faraday cage.

3. Results and discussion

3.1. Precipitate-solution equilibrium: iron (III)/hydroxide and iron (III)/benzoate

The analysis of the precipitate, obtained when benzoate anion reacted with ferric cation, revealed that there were three moles of benzoate per each mole of ferric cation; so it was concluded that the precipitate formula was $FeBz_3$ ($Fe(C_7H_6O_2)_3$).

K_{SP} of ferric hydroxide could be calculated as follow. Let V_1 be the base volume employed to titrate hydrochloric acid in the sample containing only ferric cation (Fig. 1), according to the Eq. (1).

$$H_3O^+ + OH^- \rightarrow 2\,H_2O \tag{1}$$

and V_2 the volume of base solution required to precipitate ferric cation as described the Eq. (2).

$$Fe^{3+} + 3\,OH^- \rightarrow Fe(OH)_3\downarrow \tag{2}$$

The K_{SP} of ferric hydroxide may be written as follows:

$$K_{SP}[Fe(OH)_3] = [Fe^{3+}][OH^-]^3 \tag{3}$$

and calculated by the equation:

$$K_{SP}[Fe(OH)_3] = \left[\frac{\frac{1}{3}(V_2 - V_a)M}{V_i + V_a}\right]\frac{K_W^3}{[H_3O^+]^3} \tag{4}$$

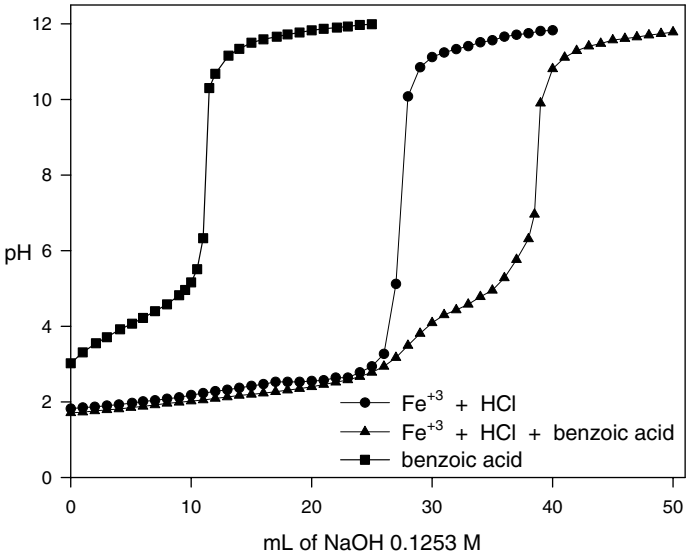

Fig. 1. Titration curves of different systems as a function of the volume of 0.1253 M sodium hydroxide.

where V_a is the base volume, corresponding, normally, to the middle point of the plateau defined when ferric hydroxide precipitated. From experimental data in Fig. 1, $V_2 = 27.50$ mL and the K_{SP} for ferric hydroxide, calculated from Eq. (4), resulted equal to 1.52×10^{-17}, being the value reported in the literature 7.50×10^{-18} [46].

The acid constant of benzoic acid was obtained from its titration curve, following the procedure described in the literature [46,47]. The calculated value was 8.04×10^{-5}; very close to that reported by Wilson, 6.30×10^{-5} [46].

The equations for ferric benzoate dissociation (Eq. (5)) and the hydrolysis of the anion (Eq. (7)) and the cation (Eq. (9)) are as follows; the constants, associated with each equilibrium, are written and calculated below.

$$Fe(Bz)_3 \Longleftrightarrow 3Bz^- + Fe^{3+} \tag{5}$$

$$K_{SP}[Fe(Bz)_3] = [Bz^-]^3[Fe^{3+}] \tag{6}$$

$$Bz^- + H_2O \Longleftrightarrow HBz + OH^- \tag{7}$$

$$K^h_{Bz} = \frac{[HBz][OH^-]}{[Bz^-]} = \frac{K_W}{K_a} \Rightarrow K^h_{Bz} = 1.24 \times 10^{-10} \tag{8}$$

$$Fe^{3+} + 6H_2O \Longleftrightarrow Fe(OH)_3 + 3H_3O^+ \tag{9}$$

$$K^h_{Fe} = \frac{[H^+]^3}{[Fe^{3+}]} = \frac{[H^+]^3[OH^-]^3}{K_{SP\ Fe(OH)_3}} = \frac{K^3_W}{K_{SP\ Fe(OH)_3}} \Rightarrow K^h_{Fe} = 1.18 \times 10^{-5} \tag{10}$$

The cation hydrolysis constant (Eq. 10) was significantly higher than that of the anion (Eq. 8). The shape of the precipitation curve in the region corresponding to ferric benzoate and the analysis of the precipitate corresponding to that portion of the titration curve, both suggested that ferric benzoate was in equilibrium with ferric hydroxide. As a consequence, K_{SP} of ferric benzoate was calculated as follows:

$$K_{SP}[Fe(Bz)_3] = [Bz^-]^3[Fe^{3+}] = \frac{K_{SP\ Fe(OH)_3}[Bz^-]}{[OH^-]^2} \tag{11}$$

The ferric benzoate K_{SP} was determined from 0.1019 M sodium benzoate solution to which the milli-moles of ferric cation, necessary to precipitate half of the amount of sodium benzoate, were added. The benzoate anion concentration in equilibrium with the precipitate was easily obtained. Then, the final pH of the system (4.19) was measured, employing a glass electrode and the concentration of hydroxyl ion to calculate ferric benzoate K_{SP} was obtained. The value of K_{SP} $[Fe(Bz)_3] = 5.25 \times 10^{-15}$ was derived from the Eq. (11) and the solubility of the compound calculated. The theoretical solubility value was found to be 1.90×10^{-4} M (54.4 ppm) while the experimental value, obtained by indirect gravimetry, was 60.2 ppm.

The foregoing discussion led to the conclusion that ferric benzoate can be easily obtained precipitating it from a slightly alkaline ammonium benzoate solution to ensure a high anion concentration and favours the ferric benzoate precipitation.

3.2. Electrochemical evaluation of ferric benzoate anticorrosive properties

At the beginning of the test, steel corrosion potential, in ferric benzoate suspension, was displaced to more negative values with respect to those attained with the supporting elec-

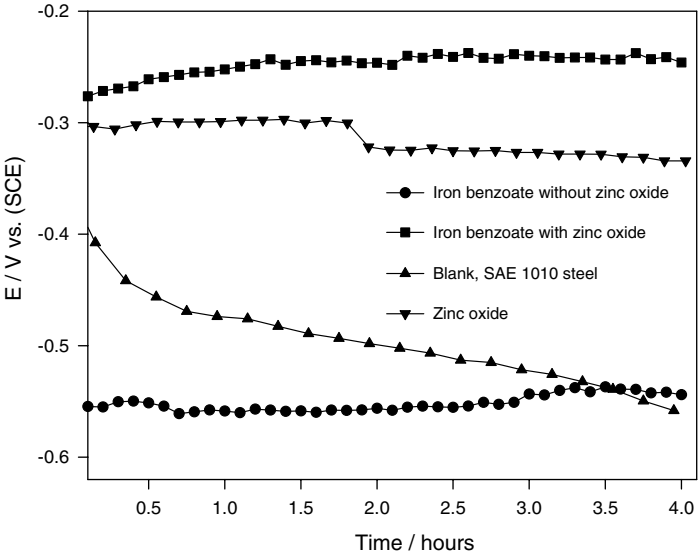

Fig. 2. Corrosion potential of SAE 1010 steel in ferric benzoate suspensions in 0.5 M $NaClO_4$.

trolyte (Fig. 2). It was thought that the acidity of ferric benzoate delayed the building of an effective protective layer, which begins to grow at pH > 7 [39]. However, certain protective properties could be perceived because steel corrosion potential did not change significantly during the test period and, finally, it was higher than steel corrosion potential in $NaClO_4$ 0.025 M. The pH of this system may be changed adding zinc oxide, a complementary pigment used in paint formulations [40]. Zinc oxide displaced the Ecorr towards more positive values, thus indicating a better protection degree. This shifting, was larger than that obtained with zinc oxide alone, was interpreted in terms of a synergism between both substances.

The SEM analysis of the protective layer formed on steel revealed that it was constituted by a uniform film with non-expansive globular formations (Fig. 3a and b). The base film and globular formations were mainly iron oxides and oxyhydroxides. It is thought that these globular formations plugged the pores and defective areas on the base metal, thus restraining the corrosion process. On the contrary, the high steel corrosion rate in ferric benzoate suspension was attributed to the presence of cracks in the continuous oxide film (Fig. 3a and b). The presence of zinc oxide in the pigment suspension modified the structure of the protective layer; a thorough uniform film, free of cracks, grew on the steel surface by causing a elevated decrease on steel corrosion rate as it will be mentioned later (Fig. 3c).

The Tafel polarization curve obtained with the SAE 1010 steel electrode in ferric benzoate suspension in 0.5 M $NaClO_4$ is depicted in Fig. 4. The cathodic current increased from 3 h (140 μA cm^{-2}) to 24 h (170 μA cm^{-2}) of exposure thus indicating a poor protection of the metallic substrate. These values were slightly lower than that obtained with a platinum electrode in the same supporting electrolyte (220 μA cm^{-2}). As it occurred with other inhibitor systems, the reduction of iron compounds forming protective layer could be taking place together with oxygen reduction [46]. Anyway, as the cathodic current on steel was lower than on the platinum electrode, it was deduced that the oxide layer

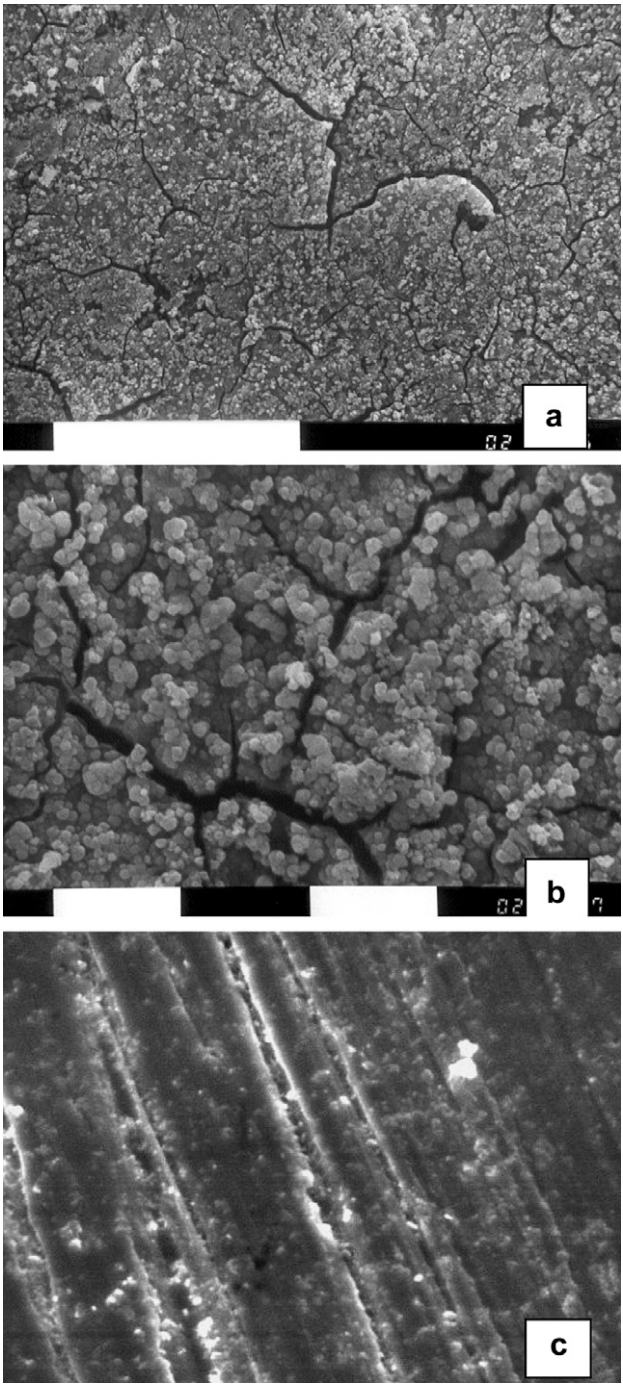

Fig. 3. SEM micrograph of the steel surface after being in contact 24 hours with ferric benzoate in suspension in 0.025 M $NaClO_4$: (a) without zinc oxide (500X); (b) without zinc oxide (2500X) and (c) with zinc oxide (2500X).

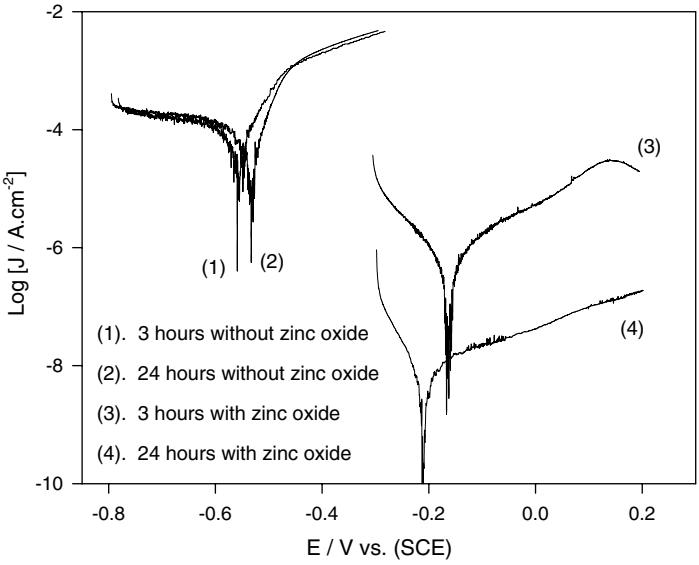

Fig. 4. Tafel plots of the SAE 1010 steel electrode in ferric benzoate suspensions in 0.5 M $NaClO_4$, at different exposure times. Swept rate 0.166 mV s^{-1}.

formed on the electrode shown a certain protective ability. The anodic branch of the Tafel polarization curve revealed that steel did not passivate in ferric benzoate suspension (Fig. 4). After 24 h of exposure the corrosion potential was displaced towards more positive values and this could be attributed to the formation of a layer with poor protective properties. Besides, the dissolution reaction appeared to be a little more polarized at low over-potentials.

In the presence of zinc oxide appeared a passivation peak at 0.15 V after three hours of exposure and the cathodic current also diminished. This behaviour was attributed to a synergism between ferric benzoate and zinc oxide which led to the formation of an effective protective layer.

Steel corrosion rate in the ferric benzoate solution, after 3 h, was found to be 95.3 μA cm^{-2} and it increased to 110 μA cm^{-2} after 24 h. The presence of zinc oxide diminished drastically steel corrosion rate to 0.77 μA cm^{-2}, after 3 h. Steel corrosion rate continued diminishing as time elapsed and was 0.73 nA cm^{-2} after one day of exposure.

3.3. Heterogeneous reaction between iron and ferric benzoate: analysis of corrosion product via spectroscopic methods

The nature of the corrosion products formed as a consequence of the heterogeneous reaction between iron and ferric benzoate was investigated by means of spectroscopic techniques, as it was said previously. UV–visible diffuse reflectance, FTIR and Mössbauer spectra of ferric benzoate and iron basic benzoate were obtained (Fig. 5) because these compounds could be formed during the corrosion reaction. UV–visible spectra were deconvoluted by adjusting the spectral curve with multiple Gaussian peaks employing the software MICROCAL ORIGIN 6.0. The fitting accuracy was assessed by means of the parameter χ^2, which was comprised between 1 and 4×10^{-5}. Bands assignment for iron

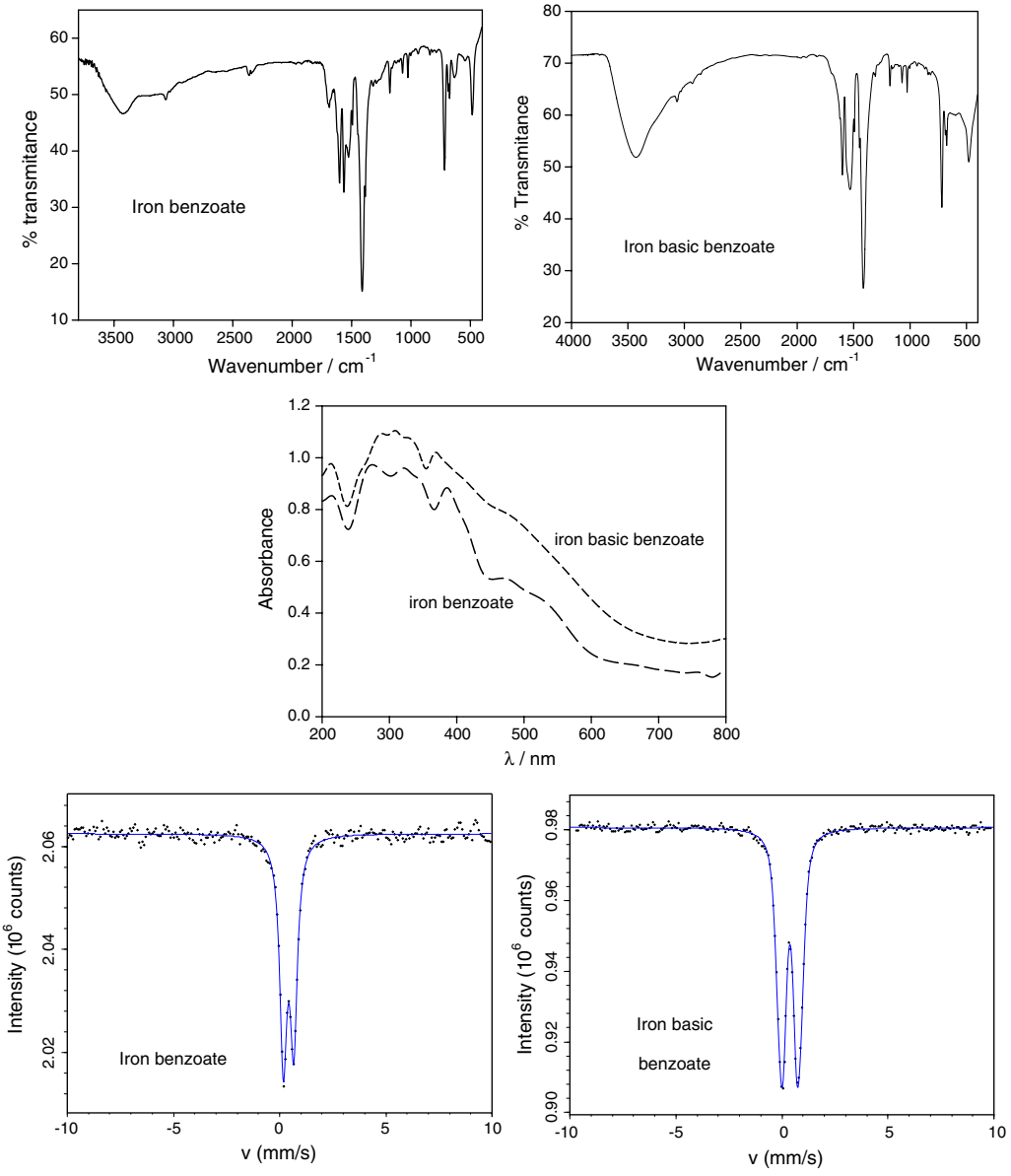

Fig. 5. UV–visible diffuse reflectance, FTIR and Mössbauer spectra of iron benzoates.

oxides and oxyhydroxides was carried out using the wavelength chart compiled by Larramona et al. [47]. Mössbauer spectra analysis was made by means of the Recoil program, employing Lorentzian lines and Voigt based methods for arbitrary shape static hyperfine parameter distribution [48].

The UV–visible spectrum of ferric benzoate exhibited several important bands at 218–224 (characteristic of benzoates), 274, 322 and 398 nm, respectively. The most important

bands of iron basic benzoate are located at 215, 287 and 371 nm. The FTIR spectrum of ferric benzoate exhibited, in the frequency group region, the following bands: 1412, 1493, 1525, 1564, 1601, 1687, 3064 and 3423 cm^{-1}. Ferric basic benzoate has a similar FTIR spectrum but it does not posses the bands located at 1493, 1566 and 1674 cm^{-1}; being the band at 1674 cm^{-1} the most intense band which could be used to differentiate both types of iron benzoate. The Mössbauer spectrum corresponding either iron benzoate or to iron basic benzoate, both had central asymmetric doublet originated by a high spin ferric compound. The most characteristic Mössbauer parameters (isomer shift and average quadrupole splitting) are different for each one. Isomer shift was 0.42 for iron benzoate and 0.38 for basic iron benzoate while the quadrupole splitting was 0.49 for the former compound and 0.81 for the last one (Table 2, Fig. 5).

The shape of the UV–visible spectra of the reaction products between iron and ferric benzoate is quite similar to that of ferric benzoate; this may be due, partially, to the existence of unreacted ferric benzoate. There was some evidence that basic ferric benzoate was formed because of the ill defined band at 1687 cm^{-1}, in the FTIR spectrum. This spectrum also confirmed the existence of ferric benzoate in the sample. The deconvolution of the UV–visible spectra revealed the absence of lepidocrocite (absorption band at 700 nm) in both mixtures [47]; FTIR measurements supported this hypothesis due to the absence of the absorption bands at 1020 and 742 cm^{-1}. The mix between iron powder and ferric benzoate contained α-FeOOH and α-Fe_2O_3; the first one being the hydrated form of the second compound. The presence of α-FeOOH was deduced by the absorption bands at 380–432 (variable width, according to particle size) and 646 nm while the existence of the anhydrous form was appreciated by the existence of the bands at 345 and 455 nm [47,49–51]. In the presence of zinc oxide the same compounds were detected. Iron oxide bands also appeared in the FTIR spectrum but, sometimes, they overlapped with those of ferric benzoate.

The Mössbauer spectrum corresponding either to the iron/ferric benzoate mixture or that also containing zinc oxide not only showed the iron sextet but also a central asymmetric doublet originated by a high spin ferric compound. This doublet was fitted as a quadrupole splitting distribution with the associated parameters calculated and presented in Table 2. There is a great variety of substances with Mössbauer parameters, at room temperature, similar to those obtained in this research. Among these compounds, lepidocrocite, super-paramagnetic goethite and amorphous oxyhydroxides could be found. This central quadrupolar doublet was finally assigned to a hydrated ferric basic benzoate ($FeBz_{3-x}OH_x \cdot nH_2O$) due to the similitude of the Mössbauer parameter values with those

Table 2
Mössbauer parameters, at room temperature, corresponding to the reaction products from iron benzoate and iron powder mixture

Sample	CS (mm/s)	$\|\Delta\|$ (mm/s)	$\sigma_{\|\Delta\|}$ (mm/s)	Γ (mm/s)	A (%)
Iron benzoate	0.42	0.49	–	0.20	100.0
Iron basic benzoate	0.38	0.81	0.28	–	100.0
M1	0.42	0.72	–	–	18.8
M2	0.38	0.69	–	0.26	19.2

CS: isomer shift with respect to α-Fe; $|\Delta|$: average quadrupolar splitting; σ: gaussian width (standard deviation) of the quadrupolar site; Γ: lorentzian width of the crystaline site; A: Site contribution to the whole spectral area; M1: molar ratio: ferric benzoate/iron: 1/1; M2: molar ratio: ferric benzoate/iron/zinc oxide: 1/1/1.

encountered for the synthesized ferric basic benzoate (Table 2). These parameters differ from the values obtained for the unidentate $Fe(C_7H_5O_2)_3$ which has an isomer shift equal to 0.40 mms^{-1} and a quadrupole splitting of 0.60 mms^{-1} [52]. So, it was concluded that basic iron benzoate was formed as a consequence of the corrosion reaction in both mixtures. However, it was difficult to say if another compound was formed, especially if its particle size fell in the nanometric scale.

The foregoing discussion pointed out corrosion products could be easily identified by UV–visible spectroscopy. Therefore the qualitative analysis of the protective layer, under the paint film, described later, was carried out only by this technique.

3.4. Painted steel panel tests

3.4.1. Accelerated tests

Results obtained in the salt spray chamber revealed that ferric benzoate is a suitable anticorrosive pigment for paints. The solvent-borne epoxy paint (paint 1) showed a very good anticorrosive behaviour up to 2130 h of exposure (0.3% of the surface rusted, qualification 7). The alkyd paint (paint 2), formulated with an intrinsically less resistant binder, attained the same qualification after 1150 h and deserved a 6 points qualification after 1400 h of exposure. The best anticorrosive behaviour was obtained with the water-borne coating (paint 3), with a very good qualification (9) after 3000 h and (7), 1000 h later (Table 3). This performance is highly satisfactory with regard to similar paints formulated with zinc phosphate [46]. These differences may be attributed not only to the binder adsorption on the steel surface but also to the inhibitive properties of ferric benzoate.

Except for the water-borne coating, which blistered after 1770 h, blistering was detected from early exposure times and did not change significantly during the whole test period. The blister surface density was low in all the cases (Table 3).

The wet adhesion of the solvent based epoxy paint maintained high values during the first 1800 h of exposure (4B, Table 4); this fact could partially explain the very good anticorrosive behaviour of the paint. After this period, adhesion fell down significantly, but the steel substrate remained protected up to 3100 h. The alkyd paint adhesion to the base metal begun to decrease after 96 h and was totally lost near to 912 h; again, steel remained protected for a longer period in spite of the adhesion loss at the paint/film interface. The water-based paint retained a high percentage of its original adhesion (4B) up to 3500 h of exposure. As it was previously said substrate protection was satisfactory during 4000 h in the salt spray test. In every case once the adhesion to the substrate was lost, the protection was mainly due to the inhibitive action of ferric benzoate.

The humidity chamber test was employed to evaluate the tendency to paint blistering. The solvent-borne epoxy paint blistered after 1770 h of exposure while the alkyd paint after 2130 h. Blisters size was small and their surface density low (Table 5). The water-borne epoxy paint blistered from the beginning of the test due to the affinity of the binder by water. In this case, blisters were initially small and of low surface density but increased in size and density as time elapsed. As a general rule, it can be said that good corrosion resistance was observed in all cases, for almost 3000 h of exposure, as a consequence of the inhibitive action of ferric benzoate.

The anticorrosive behaviour of this pigment may be compared with its predecessor, zinc phosphate. The comparison between ferric benzoate and zinc phosphate is rather complicated because there are several products in the market, each one of different quality. The

Table 3
Rusting[a] (ASTM D 610) and blistering[b] (ASTM D 714) degrees of the painted panels exposed to the salt spray chamber (ASTM B 117)

Time/hours	Paints					
	1		2		3	
	R	B	R	B	R	B
310	10	10	10	10	10	10
620	10	10	10	6F	9	10
770	10	8F	10	6F	9	10
980	10	8F	8	6F	9	10
1150	9	8F	7	6F	9	10
1400	9	6F	6	6F	9	10
1580	9	6F			9	10
1770	8	6F		–	9	10
2130	6	6F		–	9	8F
3100		–		–	9	8F
3600		–		–	8	8F
4000		–		–	7	8F
4200		–		–	6	8F

[a]R: rusting degree (ASTM D 610)

Rust grade	10	9	8	7	6	5	4	3	2	1
Rusted area/%	no rusted	0.03	0.1	0.3	1	3	10	16	33	50

[b]B: blistering degree (ASTM D 714)

Frequency	Dense, D	Medium dense, MD	Medium, M	Few, F
Size	10	8	6, 4	2
Comments	No blistering	Smaller size blister easily seen by unaided eye	Progressively larger sizes	

Table 4
Wet adhesion test[c] (ASTM D 3359) of painted panels as a function of the exposure time to the salt spray chamber (ASTM B 117)

Time/hours	Paints		
	1	2	3
0	5B	5B	5B
96	5B	4B	5B
576	4B	3B	5B
744	4B	2B	5B
912	4B	0B	4B
1176	4B	–	4B
1800	4B	–	4B
2400	3B	–	4B
3500	2B	–	4B
3800	–	–	3B

[c]Tape-test method B (ASTM D 3359)

Classification	5B	4B	3B	2B	1B	0B
Removed area/%	0	<5	5–15	15–35	35–65	>65

Table 5
Rusting (ASTM D 610) and blistering (ASTM D 714) degrees of the painted panels exposed to the humidity chamber (ASTM B 2247)

Time/hours	Paints					
	1		2		3	
	R	B	R	B	R	B
480	10	10	10	10	10	8M
1400	10	10	10	10	9	8M
1770	10	10	10	10	8	6M
2130	9	8F	9	n	8	6M
2650	8	8F	8	8F	8	6M
2890	7	8F	7	8F	8	6M
3150	7	8F	6	8F	8	6MD
3600	6	8F	–		7	6MD
4000	–		–		6	6MD

best zinc phosphate allow to obtain good results in the salt spray test after 1000 h of exposure of an alkyd paint (qualification 8), which was impaired as time elapsed (qualification 6 after 1700 h of exposure). Alkyd paints of similar composition, but pigmented with ferric benzoate, showed a very slightly worst anticorrosive performance. Epoxy paints formulated with zinc phosphate begun to fail, as an average, after 1700 h of exposure in the salt spray test while similar paints formulated with ferric benzoate underwent 2130 h in this test maintaining an acceptable degree of protection. It was reported that water-borne paints pigmented with zinc phosphate behaved satisfactorily during 2400 h of exposure in the salt spray chamber (qualification 10) [46]. Similar paints pigmented with ferric benzoate showed very good anticorrosive performance during 3100 h (qualification 9). This led to the conclusion that ferric benzoate is able to replace zinc phosphate with equal or even better behaviour.

Alkyd paints pigmented with zinc phosphate blistered after 350 h in the humidity chamber while those containing ferric benzoate showed an excellent performance beyond 2000 h of exposure. The epoxy paint formulated with ferric benzoate exhibited higher resistance to blistering which appeared after 1770 h while the process for epoxy paints formulated with zinc phosphate begun, in all cases, after 750 h of exposure. Water-borne paints formulated either with ferric benzoate or with zinc phosphate did not show resistance to blistering due to the nature of the binder which tended to re-emulsification Fig. 6.

The surface morphology of the steel panels was studied by means of SEM after removing the organic coating with suitable solvents. Xylene was employed for softening the paint film which was finally removed with THF and/or 1-Methyl-2-pyrrolidon. The protective layer formed beneath the paint films was mainly constituted, in all cases, by non-expansive iron oxides or iron oxyhydroxides (Fig. 7a and b). It is assumed that the formation of these compounds occurred because their solubility product constant is lower than that of ferric benzoate. Fig. 7a shows the protective layer formed under the alkyd paint after the exposure to the salt spray chamber. The amount of C coming from ferric benzoate was low (10.0%) and uniformly distributed across the entire surface, i.e. no special spot enriched in ferric benzoate was found. Small amounts of Si (7.3%) and Ti (1.7%) from the complementary pigments was also detected. The small prisms in the micrographs contained high

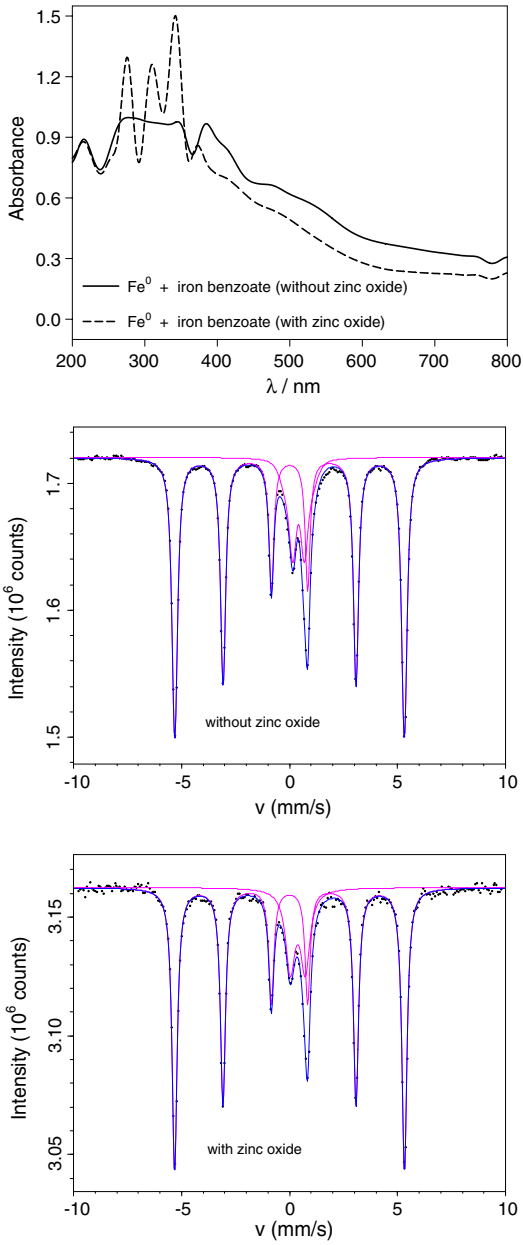

Fig. 6. UV–visible diffuse reflectance, FTIR and Mössbauer spectra of the iron/iron benzoate mixtures.

amounts of titanium. In the same micrograph the presence of pores oxide layer able to impair its protective properties.

A crystalline iron oxide layer appeared under epoxy paints (Fig. 7c). It is thought that the lower coating permeability and the pigment inhibitive action, in both types of epoxy paints restrained the corrosion process and favoured the development of these crystalline

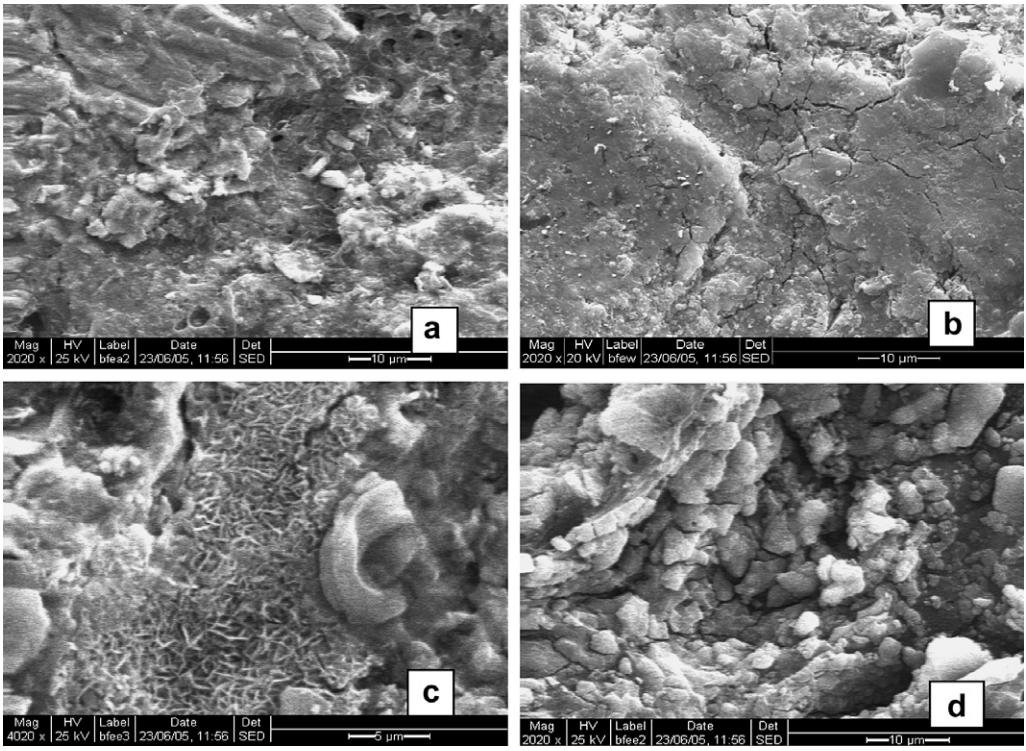

Fig. 7. SEM micrograph of the steel surface after removing the different coatings on panels exposed to the salt spray chamber (ASTM B 117). (a) alkyd paint (2000X); (b) water-borne epoxy coating (2000X), (c) solvent-borne epoxy coating (4000X) and (d) corroded area (2000X).

oxides, not observed in the case of the alkyd paint with poorer protective properties. Fig. 7d shows the protective film area, where the corrosion has started. The more or less uniform film was replaced by these globular formations which contained chlorides (up to 8.0%) and were considered as incipient corrosion spots.

The deconvolution of the UV–visible spectrum (Fig. 8) of the protective layer formed at the steel/alkyd paint interface allowed to infer the formation of α-FeOOH (goethite) due to the absorption bands at 380–432 nm (variable width) and 646 nm [47,50–52]. The presence of lepidocrocite (γ-FeOOH), as consequence of the corrosion process, was evidenced by the absorption bands at 294 and 700 nm. The existence of hematite (α-Fe_2O_3) was evidenced by the set of absorption bands located at 220, 292, 346 and 455 nm [47,50–52]. The characteristic wavelengths of ferric basic benzoate were also detected.

Corrosion products grown under the solvent-borne epoxy paint were constituted by α-FeOOH and γ-FeOOH. It was also detected the formation of α-Fe_2O_3 with the same set of bands found in the case of alkyd paints and a band at 533–566 nm with variable width. Ferric basic benzoate was also formed during the corrosion process as it could be appreciated by the absorption band at 329 nm. The band at 273 nm, attributable to ferric benzoate was also perceived (Fig. 8).

The protective layer formed just beneath the water-borne coating basically contained the alpha compounds: α-FeOOH and α–Fe_2O_3, although γ-Fe_2O_3 could be also formed.

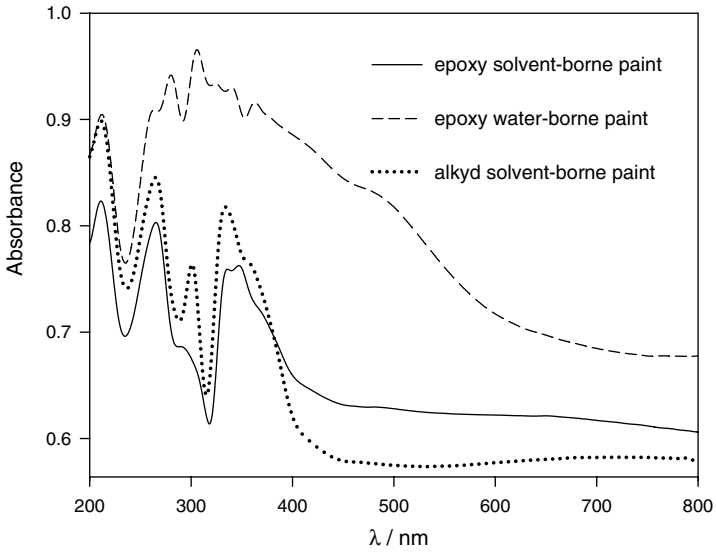

Fig. 8. UV–visible diffuse reflectance spectra of the steel surface of coated panels exposed to the salt spray, after paint removal by suitable solvents.

As in previous cases, ferric benzoate was also formed and it is thought to be the primary corrosion product; many absorption bands of this compound were detected. Oxides and oxyhydroxides are supposed to be formed as a consequence of a long exposure to corroding species.

3.4.2. Electrochemical impedance measurements

Impedance spectra give useful information concerning the evolution of both, the organic coating protective properties and the kinetics of the underlying steel corrosion process, as a function of the immersion time in the selected electrolyte. Many processes such as the dynamic nature of the membrane barrier effect, the pigments anticorrosive action, changes in the disbonded area, etc. are responsible of the variations of the coated steel/electrolyte impedance. The point of view adopted in this paper was that of Amirudin and Thierry [53] in the sense that visual observation of the spectra could not indicate the exact number of time constants involved in the degradation of the organic coating subjected to a corrosive environment, in change the number of these constants must be determined by data analysis rather than by visual observation of spectra. Fortunately, appropriate equivalent circuits have been proposed to describe the behaviour of painted metals (Fig. 8); these circuits were discussed previously by several authors [57–66]. Experimental impedance data are usually fitted with non-linear least squares algorithms, involving the transfer function derived from the equivalent circuit models, in order to obtain circuit parameters [53–56].

The impedance of a high-quality, non-defective organic coating, is that of a dielectric capacitor with a frequency dependence expressed by the Eq. (12).

$$\mathrm{Zc} = -j/\mathrm{wC} \tag{12}$$

However, as the coating degrades, an in-phase component develops as a result of shorting the organic coating capacitance with a parallel resistor. This resistor represents the development of ionic conducting paths which may occur through microscopic pores or virtual pores defined by low cross-linking regions in the polymer with concomitant high ionic transport. This model has essentially been proposed by Brasher and Nurse [62], Kendig and Leidheiser [63,64], Kendig and Scully [58], Mansfeld and Kendig [65] and Beaunier, Epelboin, Lestrade and Takenouti [66]. Thus, R_s represents the electrolyte resistance between the reference and working (coated steel) electrodes, R_1 the resistance to the ionic flux through paths short-circuiting the paint film, and C_1 the dielectric capacitance of the intact part of the same film (Fig. 9a).

Once the permeating and corrosion-inducing chemicals (water, oxygen and ionic species) reach the electrochemically active areas of the substrate, particularly the bottom of the paint film pores, metallic corrosion takes place and its associated parameters, the double layer capacitance (C_2) and the charge transfer resistance (R_2) can be obtained from the fitting procedure. It is important to remark that R_2 and C_2 values vary inversely and directly, respectively, with the size of the attacked metallic area. There is almost an unique opinion that a polymer coated metal is represented by the circuit in Fig. 9c when water penetrates the coating and reaches the metal. It is also agreed that the general impedance may include the Zd, the mass transfer (Warburg) impedance [60].

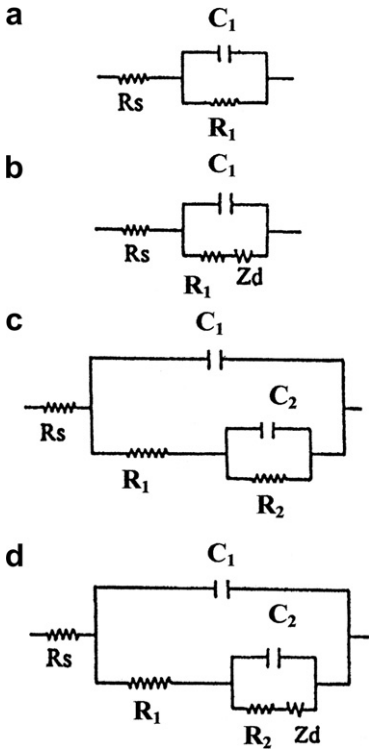

Fig. 9. The different equivalent circuits model the behaviour of organic coatings: (a) intact coating; (b) a coating with a diffusion process across it; (c) and (d) a coating where the faradaic process associated with corrosion started.

Sometimes, when the strength of the bonding forces at the paint/substrate interface are affected (e.g. by wet adhesion), facilitating lateral diffusion of the electrolyte, other processes under and/or within the intact parts of the coating could be graphically and/or numerically separated, causing the appearance of an additional time constant (R_3C_3) [67].

Distortions observed in these resistive–capacitive contributions indicate a deviation from the theoretical models due to either lateral penetration of the electrolyte at the steel/paint interface (usually started at the base of intrinsic or artificial coating defects), underlying steel surface heterogeneity (topological, chemical composition, surface energy) and/or diffusional processes that could take place along the test [68,69]. Since all these factors cause the impedance/frequency relationship to be non-linear, they are taken into consideration by replacing the capacitive components (C_i) of the equivalent circuit transfer function by the corresponding constant phase element Q_i (CPE), thus obtaining a better fit of data [45,60]. The CPE is defined by the Eq. (13), [70].

$$Z = \frac{(j\omega)^{-n}}{Y_0} \tag{13}$$

where: Z, impedance of the CPE ($Z = Z' + Z''$) (Ω); j, imaginary number ($j^2 = -1$); ω, angular frequency (rad); n, CPE power ($n = \alpha/(\pi/2)$. (dimensionless); α, constant phase angle of the CPE (rad); Y_0, part of the CPE independent of the frequency (Ω^{-1}).

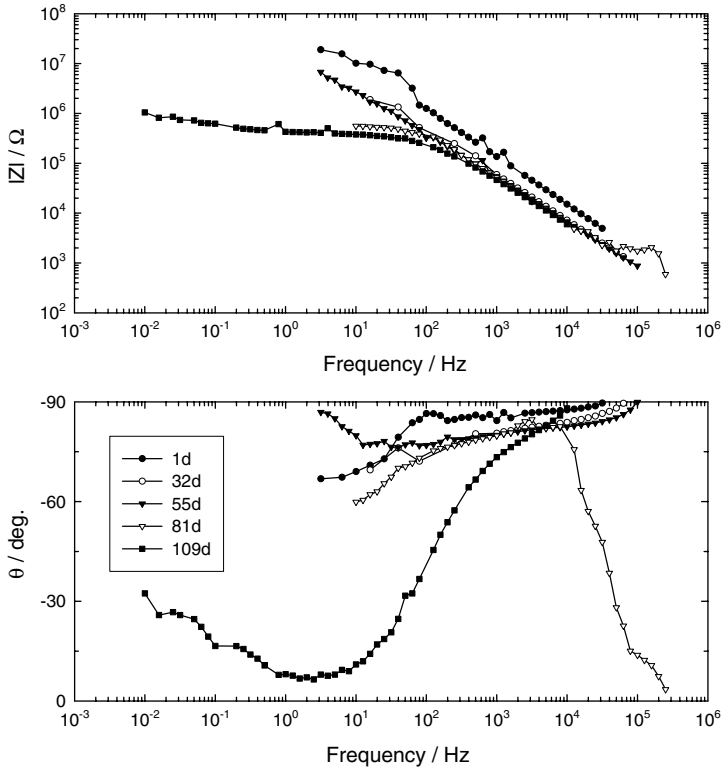

Fig. 10. Bode plots, at different exposure times, for paint 1 in 0.5 M $NaClO_4$.

The accuracy of the fitting procedure was measured by the χ^2 parameter obtained from the difference between experimental and fitted data; the most probable circuit was selected providing that $\chi^2 < 10^{-4}$.

In the present work, the fitting process was mainly performed using the phase constant element Q_i instead of the dielectric capacitance C_i. However, this last parameter was used in the plots in order to facilitate results visualization and interpretation.

The relative performance of painted steel samples, submerged in 0.5M $NaClO_4$ and 3% NaCl, was evaluated by examining Bode plots (Figs. 10–15) and, then, analysing the variation of Ecorr and R_i–C_i with the exposure time (Figs. 16–19).

The examination of Bode plot corresponding to paint 1 (solvent-borne epoxy coating, Figs. 10 and 11), in both electrolytes, revealed that the coating showed a behaviour which was predominantly capacitive during, at least, three weeks of immersion. It is also clear that more than one time constant is involved in the coating degradation process.

The analysis of Bode plot of the alkyd paint (paint 2), in both electrolytes (Figs. 12 and 13), show that the phase angle was close to 90° during the first day of immersion, thus indicating a capacitive behaviour originated in an almost intact coating. The deviation from a purely capacitive behaviour is more evident in chloride medium (Fig. 13). Beyond the first day of immersion, the existence of more than one time constant became evident as well as an important decrease in the impedance of the steel/coating system. A recovery of the

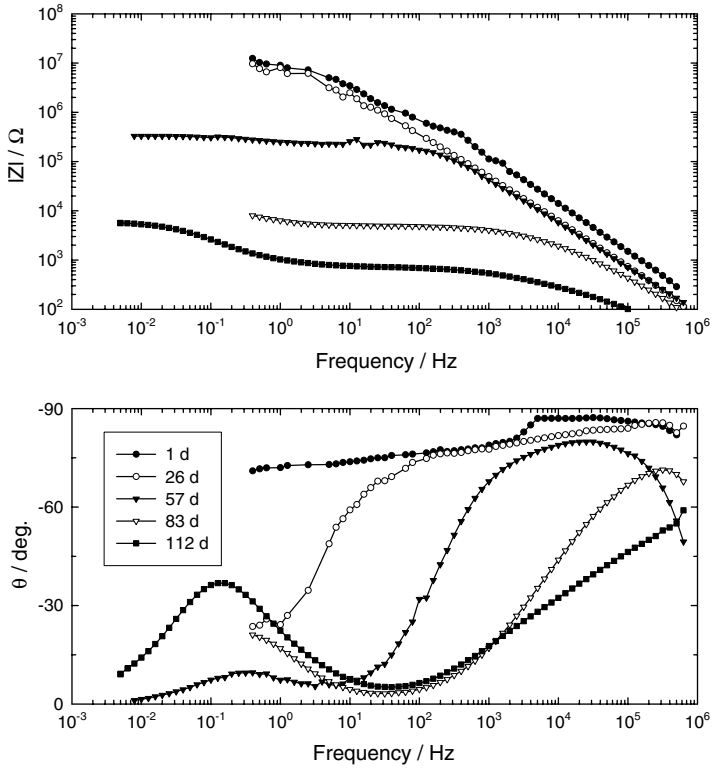

Fig. 11. Bode plots, at different exposure times, for paint 1 in 3% NaCl.

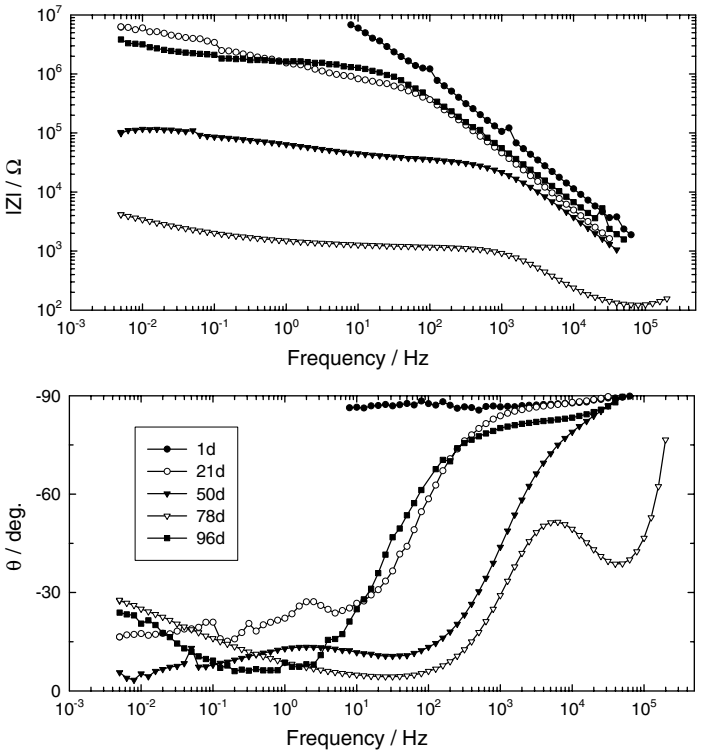

Fig. 12. Bode plots, at different exposure times, for paint 2 in 0.5 M $NaClO_4$.

barrier properties was noticed in perchlorate medium when 96 days of immersion have elapsed. This behaviour could be originated by pore blocking by corrosion products and was accompanied by the corresponding increase in the phase angle value.

Bode plots for the water-borne coating, in both electrolytes (Figs. 14 and 15), pointed out the existence of more than one time constant, too. The behaviour, as in the other cases, was predominantly capacitive during the first day of immersion. The impedance modulus was higher than 10^6 Ω during the test period and increased as time elapsed due, probably, to pore blocking by corrosion products.

As more than one time constant was involved in all impedance spectra, experimental data were fitted with the equivalent circuits presented in Fig. 9, as it was suggested by Amirudin and Thierry [60].

From a thermodynamic point of view, the epoxy paints afforded the best protective behaviour since the corrosion potential attained more positive values along the test period. Solvent-borne epoxy paint showed an interesting behaviour because the corrosion potential of coated panels could recover positive values, pointing out the substrate repassivation. The water-borne epoxy paint showed a very good behaviour for more than 100 days of immersion and, as in the other cases, the protection failed before in 3% NaCl that in 0.5 M $NaClO_4$ (Fig. 16). The corrosion potential of steel coated with the alkyd paint moved towards more negative values faster than panels with the epoxy coatings. Initially, corrosion potential values shifted to positive values, indicating that steel substrate was

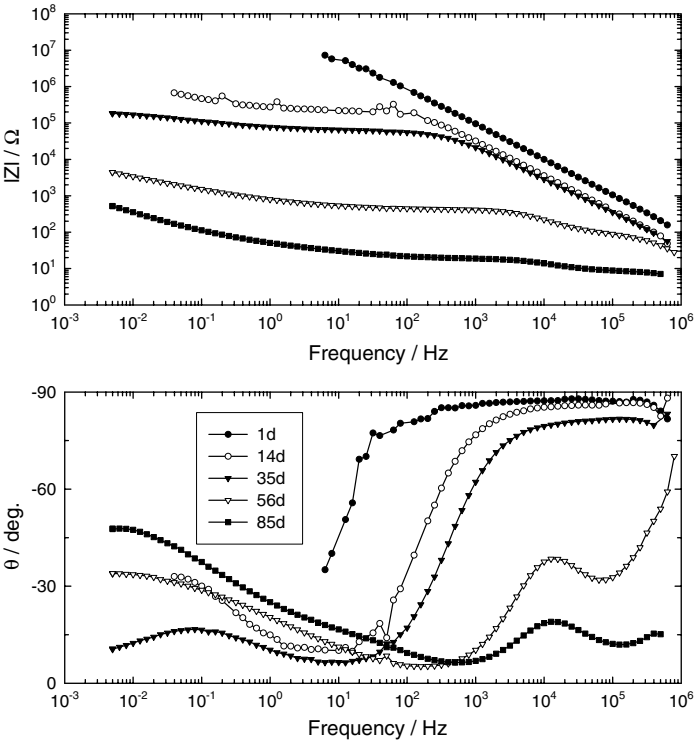

Fig. 13. Bode plots, at different exposure times, for paint 2 in 3% NaCl.

protected; but this protection disappeared after a few days in 3% NaCl and three weeks in 0.5 M $NaClO_4$. Steel repassivation may be deduced from the oscillating behaviour of this magnitude as a function of time.

The ionic resistance (R_1) of coatings pigmented with iron benzoate is initially higher than $10^7\ \Omega\ cm^2$ and, in certain cases, exceeded $10^8\ \Omega\ cm^2$ (Fig. 17). It is reported in the literature that an acceptable barrier effect is attained when $R_1 > 10^8\ \Omega\ cm^2$, and a residual protective effect is still present if R_1 ranged between 10^6 and $10^7\ \Omega\ cm^2$ [71–74]. No important differences were observed between both types of electrolytes although values in 0.5 M $NaClO_4$ were, in most cases, higher. As a general rule, the R_1 values remained higher than $10^6\ \Omega\ cm^2$ during the first 40 days of immersion, being an exception the epoxy paints in 0.5 M $NaClO_4$ which varied between 10^5 and $10^6\ \Omega\ cm^2$. This evolution was more evident in the case of alkyds which exhibited very low ionic resistance values after a few immersion days [46,75]. After this period, the ionic resistance of alkyd paints decayed significantly, thus indicating the complete absence of a barrier effect. The ionic resistance of the solvent-borne epoxy paint decreased to $10^4\ \Omega\ cm^2$ in chloride medium, although certain recovering of the barrier properties could be observed after 60 days of immersion. Again, this effect may be attributed to pore blocking by corrosion products. The water-borne epoxy paint showed a similar behaviour but after 30 days of immersion; however, beyond 300 days of immersion in both electrolytes a barrier properties enhancement, and therefore, an improvement on the anticorrosive properties could be appreciated (Fig. 17).

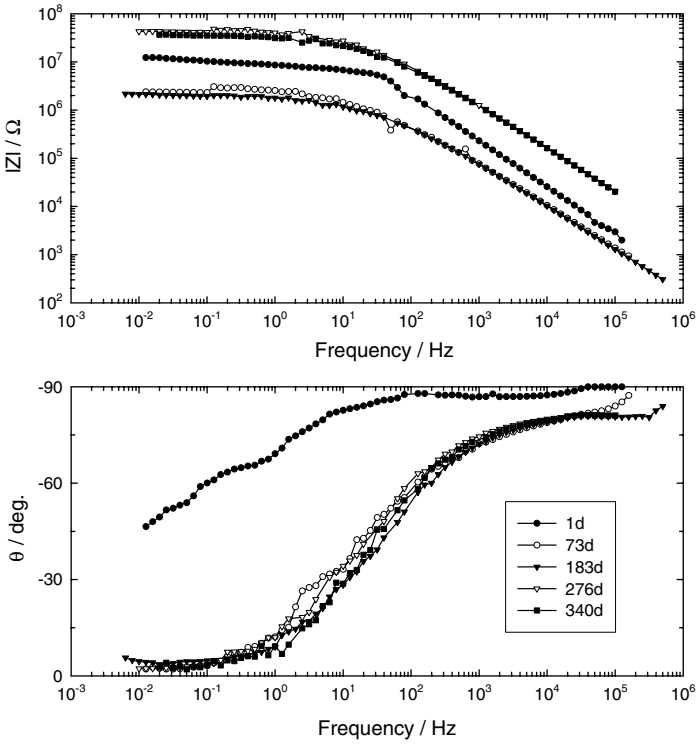

Fig. 14. Bode plots, at different exposure times, for paint 3 in 0.5 M $NaClO_4$.

The C_1 values were low up to 60 days of immersion, indicating that the coating remained intact and the volumetric fraction of permeated water was also low [71–74]. Alkyd paints showed a sudden increase after 60 days in 0.5 M NaCl and 90 days in 0.5 M $NaClO_4$ as a consequence of the film degradation. On the contrary, this process was hindered in the case of water-borne epoxy paints (Fig. 17).

The faradaic process relaxation took place in spite of the relatively high ionic resistance; so the impedance spectra deconvolution allows to detect a second time constant (R_2C_2), in many cases, from early times (Fig. 18). The beginning of this process depended on both the nature of the paint binder and the electrolyte selected to carry out the immersion test. Some paints changed from a capacitive to a mixed resistive–capacitive behaviour after three days of immersion but the faradaic process was evident in all the coated steel samples after 11 days of immersion. It is noticeable that R_2 maintained between 10^6 and 10^8 $\Omega\,cm^2$ for all paints except alkyds during, approximately, 100 days of immersion. This fact was attributed, in this case, to the inhibitive properties of ferric benzoate combined with the less important but also effective barrier effect afforded by the painting system. This is particularly noticeable with water-borne paints which showed this behaviour at longer exposure times (~400 days) in both electrolytes. The substrate repassivation was also evident at that time as well as with the solvent borne epoxy paint in the less aggressive 0.5 M $NaClO_4$; for which R_2 values $\sim 10^8$ $\Omega\,cm^2$.

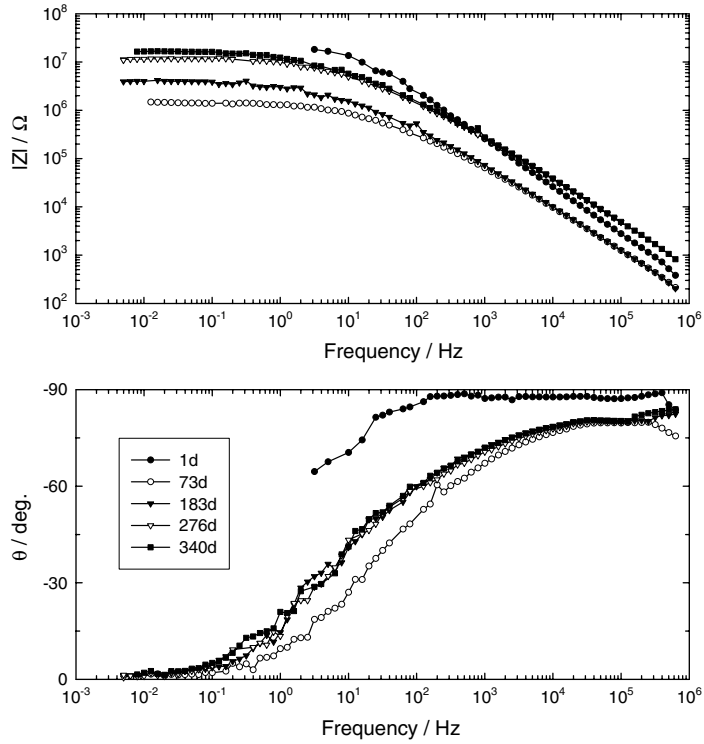

Fig. 15. Bode plots, at different exposure times, for paint 3 in 3% NaCl.

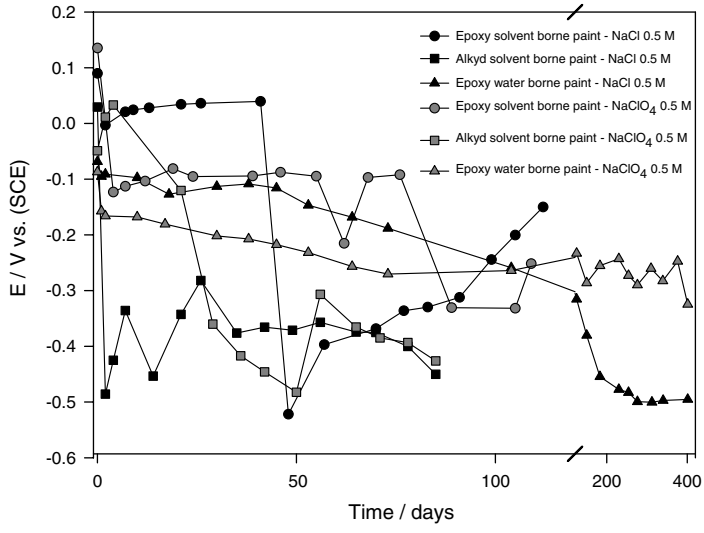

Fig. 16. Corrosion potential of coated steel in 0.5 M $NaClO_4$ and 3% NaCl.

The C_2 values of all paints are maintained below 10^5–$10^6\ \Omega\,cm^2$ during almost two months of immersion (Fig. 18). Lately, the double layer capacitance at the steel/alkyd

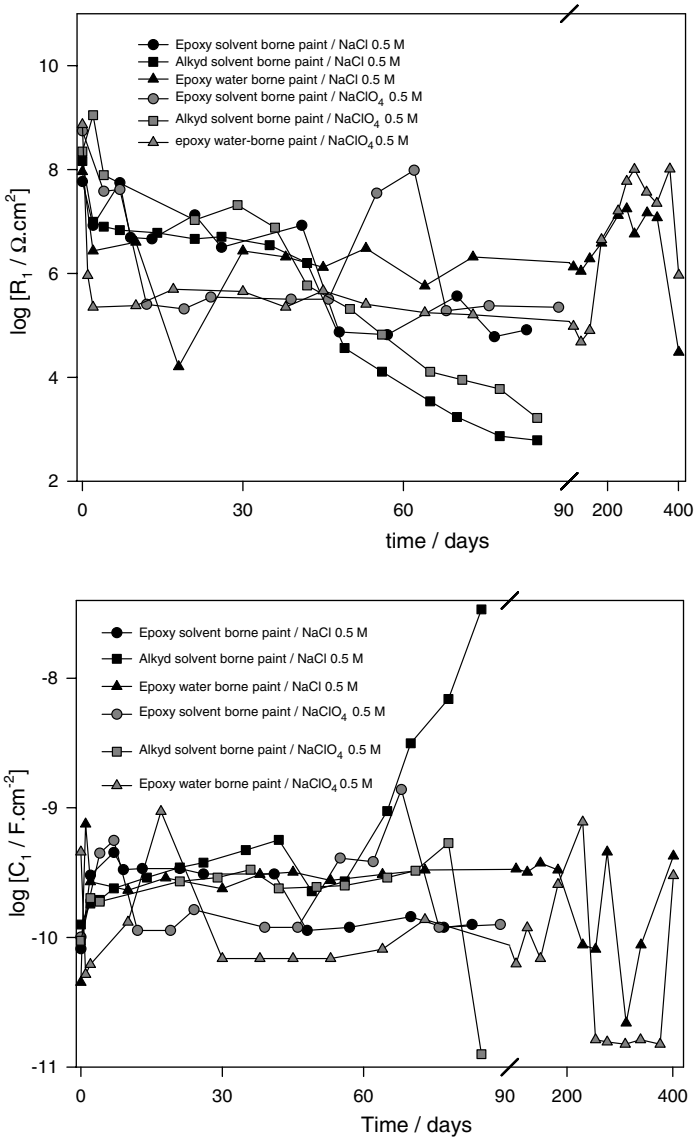

Fig. 17. Fitting parameters, R_1 and C_1, for the different coatings, as a function of the immersion time in 0.5 M $NaClO_4$ and 3% NaCl.

paint interface begun to increase as the electrochemically active area did. The rest of the painted samples showed rather low C_2 values along the test period. The oscillating behaviour of C_2 values could be attributed to dynamic changes in the surface covering degree with a protective layer of corrosion products.

As it was stated previously, the R_3C_3 time constant frequently attributed to a corrosion process taking place under delaminated areas appeared before in chloride media than in perchlorate media (Fig. 19). The corrosion under delaminated areas also depended on

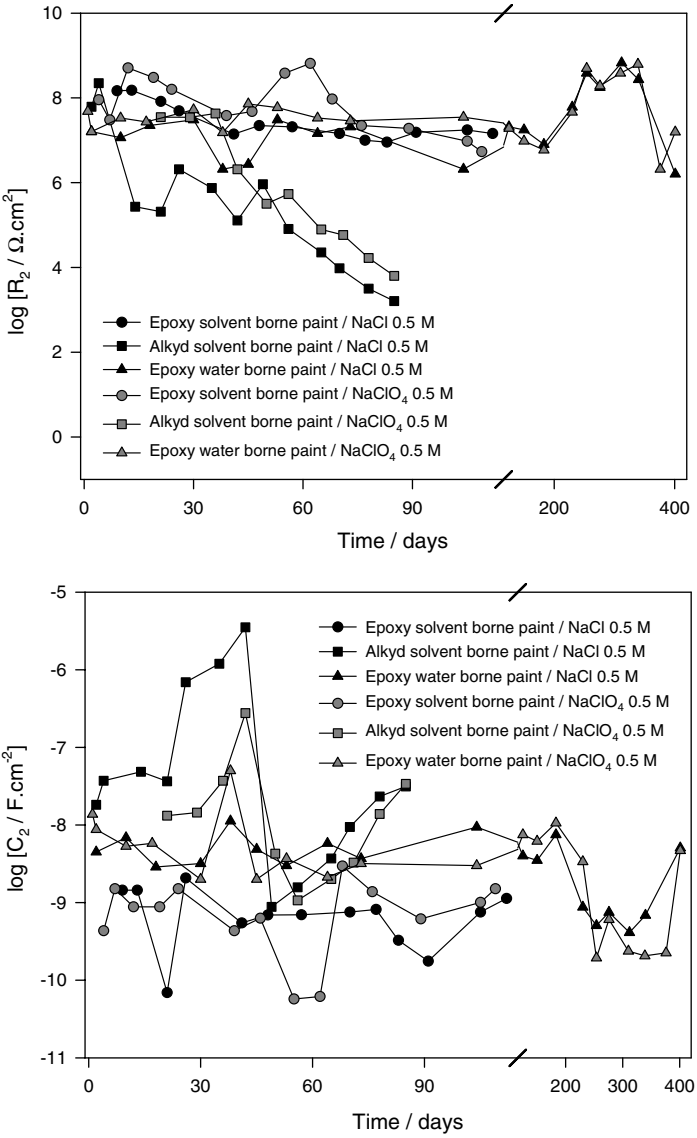

Fig. 18. Fitting parameters, R_2 and C_2, for the different coatings, as a function of the immersion time in 0.5 M $NaClO_4$ and 3% NaCl.

the binder employed to formulate the different paints. It was detected in water-borne paints from the very beginning of the test, then in alkyd paints and, lately, in epoxy paint. The charge transfer resistance maintained rather high during the test period due to the inhibitive properties of ferric benzoate, being the exception to the rule the alkyd paint. The electrochemically active area was small in all cases, except for the alkyd paints whose barrier properties were lost and the action of the pigment could not stop the corrosion process.

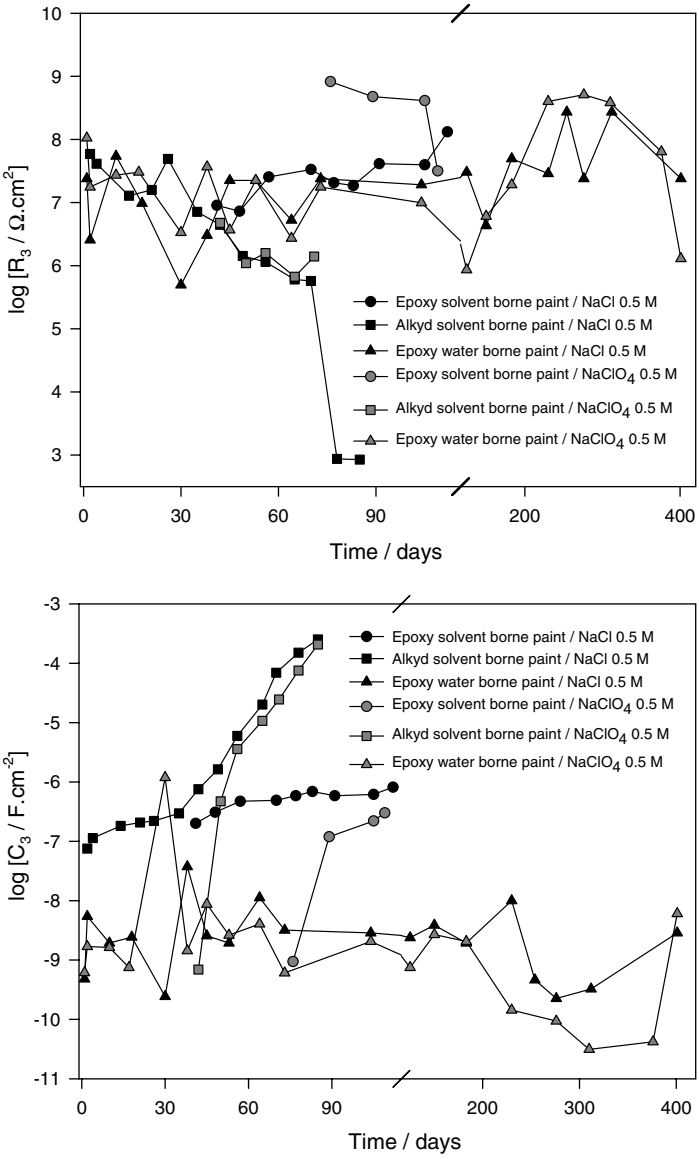

Fig. 19. Fitting parameters, R_3 and C_3, for the different coatings, as a function of the immersion time in 0.5 M $NaClO_4$ and 3% NaCl.

4. Conclusions

1. Ferric benzoate could be adequately precipitated from ammonium benzoate solution employing ferric nitrate. The pigment solubility was adequate to formulate anticorrosive paints.
2. The electrochemical tests performed with pigment suspensions confirmed the corrosion inhibiting properties of ferric benzoate.

3. The protective layer formed on steel was constituted by iron oxides or oxyhydroxides as well as iron benzoates.
4. Electrochemical test showed that ferric benzoate must be used together with zinc oxide in order to neutralize the hydrolytic acidity of the pigment.
5. Accelerated tests showed that ferric benzoate performed satisfactorily with different binders. Its anticorrosive behaviour is equal or even better than zinc phosphate, except for alkyd paints.
6. Electrochemical tests showed that the pigment action is associated with very high charge transfer resistance values, and it is the main but not the only responsible of the protection afforded by the painting systems. The barrier properties also contributed to the anticorrosive protection but they are strongly depending on the paint binder.

Acknowledgements

The authors are grateful to: CONICET (Consejo Nacional de Investigaciones Científicas y Técnicas), CICPBA (Comisión de Investigaciones Científicas de la Provincia de Buenos Aires) and UNLP (Universidad Nacional de La Plata) for their sponsorship to do this research. G. Blustein also thanks Professor F. V. Vetere for having advised on analytical topics.

References

[1] D. Eurof Davies, Q.J.M. Slaiman, Corros. Sci. 11 (1971) 671–682.
[2] Q.J.M. Slaiman, D. Eurof Davies, Corros. Sci. 11 (1971) 683–692.
[3] D. Eurof Davies, Q.J.M. Slaiman, Corros. Sci. 13 (1973) 891–905.
[4] V.S. Muralidharan, R. Sethuraman, S. Krishnamoorthy, Bull. Electrochem. 4 (1988) 705–710.
[5] D.S. Azambuja, L.R. Holzle, I.L. Muller, C.M.S. Piatnicki, Corros. Sci. 41 (1999) 2083–2097.
[6] Masahiko Yamaguchi, Hiroshi Nishihara, Kunitsugu Aramaki, Corros. Sci. 36 (1994) 241–258.
[7] Mübeccel Ergun, Ya Sar Turan, Corros. Sci. 32 (1991) 1137–1142.
[8] V. Otieno-Alego, G.A. Hope, H.J. Flitt, G.A. Cash, D.P. Schweinsberg, Corros. Sci. 33 (1992) 1719–1734.
[9] R. Kahraman, A. Al-Mathami, H. Saricimen, N. Abbas, S. Arman, A-Corros. Meth. Mat. 49 (2002) 346–353.
[10] P. Argawal, D. Landolt, Corros. Sci. 4–5 (1998) 673–691.
[11] R. Kahraman, J. Mat. Eng. Perform. 11 (2002) 46–50.
[12] K. Takahashi, J.A. Bardwell, B. MacDougall, M.J. Graham, Electrochim. Acta 37 (1992) 489–494.
[13] J.R. Culleré, M. Lluveras, Rev. Ib. Corrosión y Protección (1983) 225–228.
[14] G. Bondietti, J. Sinniger, W. Stumm, Colloids Surf. A: Physicochem. Eng. Aspect 79 (1993) 157–167.
[15] R. Kahraman, H. Saricimen, M. Al-Zahrani, S. Al-Dulaijan, J. Mater. Eng. Perform. 12 (2003) 524–528.
[16] O. Lahodny-Śarc, F. Kapor, Mater. Sci. Forum 289–292 (1998) 1205–1216.
[17] G. Blustein, J. Rodríguez, R. Romagnoli, C.F. Zinola, Corros. Sci. 47 (2005) 369–383.
[18] P.N.S. Yadav, A.K. Singh, R. Wadhwani, Corros. NACE 55 (1999) 937–941.
[19] A. Raspini, Corros. NACE 49 (1993) 821–828.
[20] A.K. Mohamed, S.A. Abd El-Maksoud, A.S. Fouda, Portugaliae Electrochim. Acta 15 (1997) 27–38.
[21] Sibel Zor, Turk J. Chem. 26 (2002) 403–408.
[22] W.J. Rudd, J.C. Scully, Corros. Sci. 20 (5) (1980) 611–631.
[23] Kanitsugu Aramaki, Corros. Sci. 43 (2001) 1985–2000.
[24] S.M. Abd El Haleem, A.A. Abdel Fattah, Surf. Coat. Tech. 29 (1986) 41–49.
[25] S. Mostafa, M. Mourand, S. Seliman, J. Electroanal. Chem. 130 (1981) 221–228.
[26] G. Blustein, C.F. Zinola, J. Colloid Interf. Sci. 278 (2004) 393–403.
[27] P. Kern, D. Landolt, Electrochim. Acta 47 (2001) 589–598.
[28] C. Monticelli, A. Frignani, G. Trabanelli, Cement Concrete Res. 30 (2000) 635–642.
[29] J. Gaidis, Cement Concrete Comp. 26 (2004) 181–189.

[30] F. Galliano, D. Landolt, Prog. Org. Coat. 44 (2002) 217–225.
[31] S.A. Hodges, W.M. Uphues, M.T. Tran, Surf. Coat. Int. 4 (1997) 178–183.
[32] C. Simpson, Paint Coat. Ind. (1993).
[33] M.A. Jackson, J. Protective Coat. Lignin (1990) 54–64.
[34] A. Kalendová, Prog. Org. Coat. 44 (2002) 201–209.
[35] Halox® Flash-X330, Halox Flash Rust Inhibitors.
[36] G. Pollano, A. Lurier, Paint Coat. Ind. May–June (1987) 15–32.
[37] I. Chet, P. Asketh, R. Mitchell, Appl. Microbiol. 30 (1975) 1043–1045.
[38] M. Stupak, M. García, M. Pérez, Int. Biodeter. Biodegr. 52 (2003) 49–52.
[39] Z. Szklarska-Smialowska, R.W. Staehle, J. Electrochem. Soc. 121 (11) (1974) 1393–1401.
[40] M.C. Deyá, R. Romagnoli, B. Del Amo, Corros. Rev. 22 (2004) 1–17.
[41] A. Gerhard, A. Bittner, J. Coat. Tech. 58 (1986) 59–65.
[42] A. Bittner, J. Coat. Tech. 61 (1984) 114–118.
[43] C.A. Giúdice, J.C. Benítez, V.J.D. Rascio, J. Oil Col. Chem. Assoc. 63 (1980) 153–158.
[44] S. Gee, Surf. Coat. J. 80 (1997) 316–322.
[45] B.A. Boukamp, Report CT88/265/128, CT89/214/128, University of Twente, The Netherlands, 1989.
[46] G. Blustein, M.C. Deyá, R. Romagnoli, B. del Amo, Appl. Surf. Sci. 252 (2005) 1386–1397.
[47] G. Larramona, C. Gutiérrez, J. Electrochem. Soc. 136 (1989) 2171–2178.
[48] D.G. Rancourt, J.Y. Ping, Nucl. Instr. Meth. B58 (1991) 85–97.
[49] R.V. Morris, H.V. Lauer, C.A. Lawson, E.K. Gibson Jr., G.A. Nace, C. Stewart, J. Geophys. Res. 90 (1985) 3126–3129.
[50] R.G.J. Strens, B.J. Wood, Mineral Mag. 43 (1979) 347–352.
[51] S.P. Tandon, J.P. Gupta, Spectros. Lett. 3 (1970) 297–305.
[52] P.S. Bassi, B.S. Randhawa, H.S. Jamwal, Termochim. Acta 69 (1983) 367–374.
[53] O. Ferraz, E. Cavalcanti, A.R. Di Sarli, Corros. Sci. 37 (1995) 1267–1280.
[54] P.R. Seré, D.M. Santágata, C.I. Elsner, A.R. Di Sarli, Surf. Coat. Int. 3 (1998) 128–134.
[55] D.M. Santágata, P.R. Seré, C.I. Elsner, A.R. Di Sarli, Prog. Org. Coat. 33 (1998) 44–54.
[56] P.R. Seré, A.R. Armas, C.I. Elsner, A.R. Di Sarli, Corros. Sci. 38 (1996) 853–866.
[57] F. Mansfeld, Corrosion (NACE) 36 (1981) 301–307.
[58] M. Kendig, J. Scully, Corrosion 46 (1990) 22–29.
[59] T. Szauer, Prog. Org. Coat. 10 (1982) 171–183.
[60] A. Amirudin, D. Thierry, British Corros. J. 30 (1995) 128–134.
[61] A. Miszczyk, H. Szalinska, Prog. Org. Coat. 25 (1995) 357–363.
[62] D. Brasher, T.J. Nurse, J. Appl. Chem. 9 (1959) 96–105.
[63] H. Leidheiser Jr., M.W. Kendig, Corrosion 32 (1976) 69–76.
[64] M.W. Kendig, H. Leidheiser, J. Electrochem. Soc. 123 (1976) 982–989.
[65] F. Mansfeld, M. Kendig, in: C. Haynes, R. Baboian (Eds.), ASTM Publication STP 866, ASTM, Philadelphia, PA, 1985, pp. 122–142.
[66] L. Beaunier, I. Epelboin, J.C. Lestrade, H. Takenouti, Surf. Technol. 3 (1976) 237–254.
[67] C. Gabrielli, M. Keddam, O.R. Mattos, H. Takenouti, J. Electroanal. Chem. 117 (1981) 147–153.
[68] T. Szauer, A. Brandt, J. Oil Col. Chem. Assoc. 67 (1984) 13.
[69] D.J. Frydrych, G.C. Farrington, H.E. Townsend, in: M.W. Kendig, H. Leidheiser Jr., (Eds.), Corros. Protection by Organic Coatings, The Electrochem. Soc., 87, Pennington, NJ, 1987, pp. 240.
[70] E.P.M. van Westing, G.M. Ferrari, F.M. Geenen, J.H. W van de Wit, Prog. Org. Coat. 23 (1993) 89–103.
[71] J.V. Standish, H. Leidheiser Jr., Org. Coat. Plastics Chem. 43 (1980) 565–569.
[72] T. Szauer, Prog. Org. Coat. 10 (1982) 171–183.
[73] C.I. Elsner, A.R. Di Sarli, Braz. Chem. Soc. 5 (1994) 15–18.
[74] H. Leidheiser, Prog. Org. Coat. 7 (1979) 79–104.
[75] G. Blustein, B. del Amo, R. Romagnoli, Pig. Res. Tech. 29 (2000) 100–107.